IEEE Access
Multidisciplinary ⋮ Rapid Review ⋮ Open Access Journal

Received November 30, 2020, accepted January 5, 2021, date of publication January 14, 2021, date of current version January 22, 2021.

Digital Object Identifier 10.1109/ACCESS.2021.3051614

Borehole Strain Observations Based on a State-Space Model and ApNe Analysis Associated With the 2013 Lushan Earthquake

ZINING YU[1,2], KAIGUANG ZHU[1,2], KATSUMI HATTORI[3], (Member, IEEE), CHENGQUAN CHI[4], MENGXUAN FAN[1,2], AND XIAODAN HE[1,2]

[1]Key Laboratory of Geo-Exploration Instrumentation, Ministry of Education, Jilin University, Changchun 130061, China
[2]College of Instrumentation and Electrical Engineering, Jilin University, Changchun 130061, China
[3]Graduate School of Science, Chiba University, Chiba 263-8522, Japan
[4]School of Information Science and Technology, Hainan Normal University, Hainan 571158, China

Corresponding author: Kaiguang Zhu (zhukaiguang@jlu.edu.cn)

This work was supported by the National Natural Science Foundation of China (Zhu K. G.) under Grant 41974084, and the Ministry of Education, Culture, Sports, Science and Technology (MEXT) of Japan, under its Observation and Research Program for Prediction of Earthquakes and Volcanic Eruptions.

ABSTRACT YRY-4 borehole strainmeters have been installed in Sichuan Province, China, since 2008, aimed at monitoring the crustal activities associated with earthquakes. In this study, data from six YRY-4 strainmeters at the southwestern endpoint of the Longmenshan fault zone were analysed, to study the relationship of tectonic strain changes with the 2013 Lushan earthquake. We developed a state-space model to remove the strain response due to air pressure, solid tides and the changes in the water level to preferentially isolate non-tectonic disturbances. Strain responses to each influencing factor were estimated using the environmental coefficients computed in the state-space model by an adaptive Kalman filter with measurement noise. The results were consistent with the expected response of the strainmeter systems. The corrected strain considered to originate from underground tectonics provides new insights into the changes in the pre-earthquake strain. Approximate negentropy (ApNe) and *b* value were introduced to quantify the probability distribution of the corrected borehole strain and compared with the local seismic activities. The nearest station and two further stations, almost simultaneously recorded short-term ApNe anomalies six to four months before the earthquake. The anomalous region also had a correspondingly low *b* value. Moreover, the anomaly acceleration rates of each station were dependent on the epicentral distances. Further comparison with the strain of random periods illustrated the significance of the extracted anomalies. Our results indicate that the corrected strain may contain seismogenic information and reflect the accelerated strain accumulation of focal areas before the earthquake.

INDEX TERMS State-space model, Kalman filter, ApNe, *b* values, short-term strain anomalies, Lushan earthquake.

I. INTRODUCTION

The preparatory process and occurrence of a major shallow earthquake are typically accompanied by crustal deformation [1], [2] (e.g., the 2011 Tohoku earthquake [3] and the 2004 Kii Peninsula earthquake in Japan [4]). Deformation data obtained by available geodetic means have now been widely used in studies on crustal motion and earthquake monitoring [5]–[10]. Among them, borehole strainmeters, which detect crustal changes at high resolution on different time scales ranging from seconds to years [11], [12] provide an opportunity to investigate the preparation process prior to earthquakes [13]–[16], slow earthquakes [17], [18], seismic strain steps [19], [20], and volcanic eruptions [21].

The 2013 Ms 7.0 Lushan earthquake is the second earthquake of magnitude 7.0 or higher that has occurred along the Longmenshan fault zone in Sichuan Province, China, after the 2008 Ms 8.0 Wenchuan earthquake. Recently, significant attention has been paid to the characteristics of whether the earthquake generation process can be recorded with geodetic

The associate editor coordinating the review of this manuscript and approving it for publication was Stefania Bonafoni.

data [9], [22]–[24]. For sequences of observations that can be used to monitor the changes in underground deformation, Chi *et al.* [25] detected anomalies in the YRY-4 borehole strain by investigating the principal stress direction deduced from the abnormal strain excluding the interference from teleseismic waves and human factors. According to their results, anomalies occurred for six to four months and four days before the Lushan earthquake from the nearest GZ station to the epicentre. Later, Yi *et al.* [26] and Zhu *et al.* [27] respectively used wavelet analysis and principal component analysis to confirm that the anomalies at the GZ station were preceded by the Lushan earthquake; However, environmental disturbances were not excluded from the borehole strain data in their studies.

Borehole strainmeters, with resolutions of less than one part per billion, increase the difficulties associated with capturing tectonic strain signals because environmental factors severely affect the identification of the changes in strain caused by crustal deformation [28]–[30]. Air pressure acting on the Earth's surface can produce crustal deformation of 10^{-9} [31], [32]. Water levels and rainfall are other important factors that can affect the local strain [28], [33], [34]. In addition, solid tidal strains typically occur as external strains, which can be used to analyse the tidal effects from borehole strainmeters [35], [36]. Strainmeters often simultaneously record the changes in the strain from multiple external influencing factors and tectonic plate movements. Thus, to extract tectonic anomalies from deformation observations, the non-tectonic disturbances should be isolated.

Numerous types of geophysical data are considered random processes. For a random process, the probability distribution of the observational data is an informative technique to extract potential anomalies in earthquake generation processes. For example, the slipping of two rough and rigid Brownian-motion-type profiles, i.e., one over the other, may generate the candidate electromagnetic precursors [37]. Manshour *et al.* [38] extracted the variance anomalies of the probability density of the Earth's vertical velocity increments and observed a pronounced transition from a Gaussian distribution to a non-Gaussian distribution prior to 12 earthquakes. Before the 2008 Wenchuan earthquake, high-frequency fluid observational data deviated from the Gaussian distribution at 16 fluid stations [39], and skewness and kurtosis (the third- and fourth-order moments) were applied to the geoelectric data to determine the non-Gaussian distribution anomalies for predicting the impending large earthquakes in Taiwan [40]. Therefore, previous studies have implied that precursor anomalies can lead to an unusual distribution in the strain data. In this study, we applied negentropy based on high-order moments to quantify the strain distribution and illustrate the temporal changes in the strain.

In this work, we analysed the data from six stations selected at the southwestern endpoint of the Longmenshan fault zone, in combination with the results of the previous deformation studies [22], [24]. To confirm the existence of the borehole strain anomalies preceding the 2013 Lushan earthquake, this is the first study to undertake a strain responses analysis to distinguish whether the changes in the strain are due to the environmental disturbance factors or tectonic motions. We developed a state-space model for the YRY-4 borehole strain data. The model is a comprehensive and straightforward method used to deconstruct the strain into its component responses to each influencing factor. Using this model, we removed the strain responses from the environmental disturbances for the observed strain via a regression model with coefficients estimated using a Kalman filter adaptive to dynamic measurement noise. We then calculated the approximate negentropy (ApNe) of the daily corrected strain and b value to quantify the probability distribution of the strain data and to compare with the local seismicity. Finally, we extracted the ApNe anomalies at six observation points to further discussion. The importance and advance of this study are that we explored the strain anomalies from the multiple observations around the focal area and provided several comparative analyses to confirm the pre-earthquake anomalies in the same area. It is hoped that this research will contribute to a deeper understanding of the relationship between the strain anomalies and the earthquake in time and space.

II. OBSERVATIONS AND DATA

A. BOREHOLE STRAIN DATA

The Lushan earthquake, with a magnitude of Ms 7.0, was a thrust earthquake that occurred at 08:02 on 20 April, 2013 in Lushan County, Sichuan, China (http://www.globalcmt.org/). The epicentre of the Lushan earthquake was located at 30.28°N, 102.94°E, with a focal depth of 13 km according to the China Earthquake Networks Center of the China Earthquake Administration. We selected six YRY-4 strainmetes from near to far south of the epicentre from 2011 to 2014 to revisit the evolution of the earthquake. These stations are generally considered to be inside the acceptable range for changes in the strain [41]. Figure 1 and Table 1 provide the details on these stations.

TABLE 1. List of borehole strain stations shown in Fig. 1.

Station Name	Geographic Coordinates	Installation Depth (m)	Rock Type	Epicentre Distance (R/km)
GZ	30.11°N, 102.17°E	41.00	Granodiorite	77
XM	28.00°N, 102.00°E	45.35	Siltstone	270
ZT	27.32°N, 103.73°E	45.00	Basalt	338
RH	26.51°N, 101.74°E	61.50	Quartz diorite	436
YS	26.69°N, 100.76°E	43.00	Sandstone	452
TC	25.02°N, 98.54°E	45.00	Andesite basalt	728

YRY-4 borehole strainmeters have been deployed at depths of more than 40 m throughout China. These strainmeters have four gauges arranged at 45° intervals, with the capability of resolving strain changes of less than one part per billion. This arrangement produces four observation values: S_i, $(i = 1, 2, 3, 4)$ [42]. Gauge i in the cylinder directly measures the change in the diameter of the corresponding azimuth, θ_i, which results from changes in the strain state. The relationship between the measurement, S_i, and changes

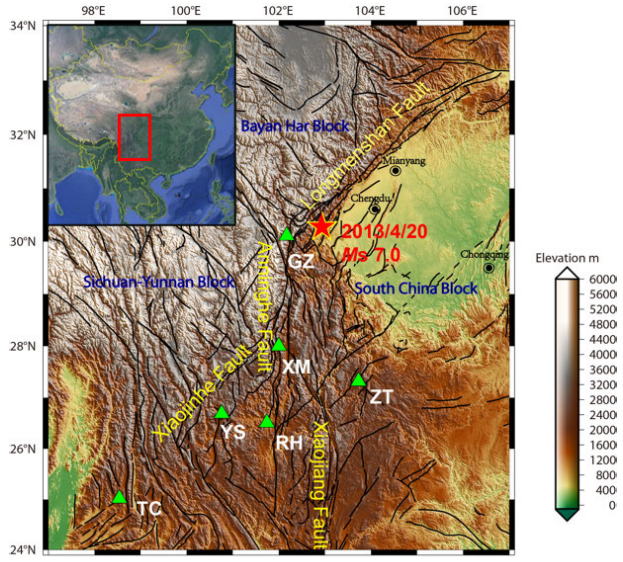

FIGURE 1. Location map showing the epicentre and six borehole strain observation points. The region under study is displayed in the indexing figure to the upper left. The epicentre was located at 30.28°N and 102.94°E. The green triangles show the observation points in the study area. The black curves indicate the faults.

in the strain $(\varepsilon_1, \varepsilon_2, \varphi)$ can be expressed as follows:

$$S_i = A(\varepsilon_1 + \varepsilon_2) + B(\varepsilon_1 - \varepsilon_2)cos2(\theta_i - \varphi), \tag{1}$$

where ε_1 and ε_2 are the maximum and minimum principal strains, respectively, and φ is the principal orientation. Two parameters, i.e., A and B, known as the coupling coefficients, are physically determined by the elastic properties of the materials involved and the geometry of the two-ring measuring system [43]. In this case, we used areal strain, S_a, and shear strain, S_s to describe the subsurface strain state instead of the four component observations. Here, S_a and S_s can be expressed as follows [42]:

$$\begin{cases} S_a = 2A(\varepsilon_1 + \varepsilon_2) \\ S_s = \sqrt{s_{13}^2 + s_{24}^2} = 2B(\varepsilon_1 - \varepsilon_2), \end{cases} \tag{2}$$

where

$$\begin{cases} S_{13} = S_1 - S_3 \\ S_{24} = S_2 - S_4 \\ S_a = (S_1 + S_2 + S_3 + S_4)/2. \end{cases} \tag{3}$$

Equation 2 is often used to derive the inversion, known as the absolute in situ calibration. The sampling rate of the strainmeters is one sample per minute.

B. ENVIRONMENTAL MEASUREMENTS

In strain-monitoring networks, air pressure and water level are synchronously maintained at every borehole with the same sampling rate, for use in comparative analyses. In this work, co-located measurements were analysed at each station. Air pressure and water level data were not available at XM and RH stations and thus were replaced by those of the ZT station. The rainfall data were downloaded through NASA GIOVANNI-4 on a 0.1° latitude 0.1° longitude grid measured by the Tropical Rainfall Measuring Mission (TRMM) satellite (http://giovanni.gsfc.nasa.gov/giovanni/).

C. EARTHQUAKE DATA

We used the earthquake catalogues issued by the China National Earthquake Data Center (http://data.earthquake.cn/) from 2011 to 2014. The study area is located at 27°N-32°N and 100°E-106°E. We selected shallow earthquakes (with a depth of 0–60 km) that occurred during the study period. The 2013 Lushan earthquake was the only earthquake of magnitude 7.0 or greater during the study period.

III. DATA PROCESSING

A. CORRECTIONS FOR ENVIRONMENTAL DISTURBANCES

To eliminate the possibility that the changes in the strain occur due to the environmental disturbances, we applied a state-space model to analyse the observed strain data, including the areal strain S_n^a and shear strain S_n^s, by assuming that the induced strain from solid tides, E_n, air pressure, P_n, and water level, W_n are additive. The state-space model can be expressed as follows:

$$\begin{aligned} S_n^a &= S_n^{ca} + E_n + P_n + W_n + \varepsilon_n \\ S_n^s &= S_n^{cs} + E_n + W_n + \varepsilon_n \\ \varepsilon_n &\sim N(0, R), \quad n = 1, 2, \ldots, N_1 \end{aligned} \tag{4}$$

where S_n^{ca} and S_n^{cs} are the corresponding corrected strain changes, ε_n is the Gaussian noise with zero mean and covariance of R, and N_1 is the length of the observations. As the air pressure does not depend on the direction, we ignored the air pressure loading in the state-space model of the shear strain. Here, E_n, P_n, and W_n are considered to be the time series related to theoretical solid tide e_n, air pressure p_n, and water level w_n, respectively, in the current and the past moments:

$$E_n = \sum_{i=0}^{l} a_i e_{n-i} \tag{5}$$

$$P_n = \sum_{i=0}^{m} b_i p_{n-i} \tag{6}$$

$$W_n = \sum_{i=0}^{k} c_i w_{n-i} \tag{7}$$

where l, m, and k are the orders for the earth tides, air pressure, and water level, respectively, and $a_0, \ldots, a_l$, $b_0, \ldots, b_m$, and $c_0, \ldots, c_k$ are the state vectors, indicating the tidal, air pressure, and water level responses, respectively. We used the Kalman filter adaptive to measurement noise to analyse the state-space model, which is described in the Appendix A, and recursively computed the optimal state vectors. The strain data and these environmental data were subsampled into hourly values. Then, we obtained the corrected strain and a series of environmental parameters, i.e.,

a_i, b_i, c_i. These parameters are related to the response of the strainmeter system and help the assessment of the installation of the sensors or the quality of the mathematical inversion.

B. APPROXIMATE NEGENTROPY OF THE CORRECTED STRAIN

In the analysis of the state-space model, the corrected strain, s_n^c, is assumed to change gradually and satisfy the random walk model [34]. We used a detection method that quantifies the probability distribution of the incremental time series, y_n, which is defined as $y_n = s_n^c - s_{n-1}^c$. Then, we detected the distribution of the daily incremental signal of the corrected strain by using a high-order statistical parameter, i.e., Approximate negentropy (ApNe). Appendix B describes the details of ApNe. ApNe is an easily computable measure of the non-Gaussian distribution used to obtain evidence of the strain changes that lead to the point of instability [44], [45]. It is note the hourly strain data were interpolated to one-minute increments to improve the robustness of ApNe. The Gaussian process has the largest entropy (minimum negentropy); thus, we consider the Gaussian process as the most random and most unorganized process. We assume that when external energy flows in the seismic system [46], the stability of the process will decrease, the signal will show organisation, and entropy will decrease, i.e., negentropy will increase.

C. B VALUE CALCULATION

The b value in the Gutenberg-Richter relationship is a widely reported seismicity parameter to detect the physical processes of stress evolution and crack growth. The b value is inversely proportional to the stress accumulation level [47]. Seismologists have attempted to use the b value to locate the locked area of a subduction zone to identify the potential source location of a large earthquake [48]. Several studies have demonstrated the possible decrease in the b value prior to large earthquakes, such as the 2008 Ms8.0 Wenchuan earthquake in China [49], the 2011 Mw 9.0 Tohoku earthquake in Japan [50], and the 2003 Tokachi earthquake [51].

As both the b value and strain data reflect the tectonic activities, a comparison of the two measurements would provide a more realistic interpretation. The b value can be computed using the maximum likelihood method [51]:

$$b = \frac{1}{ln(10)(M - Mc)}, \tag{8}$$

where M denotes the average magnitude with $M \geq Mc$ in a moving window and Mc is the corresponding magnitude of completeness. We also provide the confidence limit of the estimated b value using $\sigma_b = b/\sqrt{N_2}$, where N_2 is the number of events with magnitudes greater than Mc [52]. We computed the temporal variations in the b value derived by a moving window of 500 samples, with a 20-sample step size. To compute the Mc within the window, we randomly sampled a dataset of 500 events out of all the earthquake events and then applied the maximum curvature (MAXC) technique [53]. We averaged the results of 1,000 repetitions as the Mc of the window.

IV. ENVIRONMENTAL RESPONSES OF THE STRAINMETER SYSTEMS

The responses of the environmental disturbances were analysed based on the results in Table 2. Table 2 lists the environmental parameters in the state-space model. Figure 2 (a) and (b) show the raw and corrected areal strain observed at the GZ station.

TABLE 2. Environmental parameters in the state-space model.

	Station Name (abbr)	GZ	XM	ZT	RH	YS	TC
Earth Tide	a0_areal	1.11	2.10	1.47	2.60	2.74	1.46
	a0_shear	2.89	4.13	4.07	4.75	3.75	3.48
Air pressure	order	18	11	9	13	14	11
	b0	-1.08	-3.03	-1.58	-1.03	-1.76	-1.56
	b1	-0.98	-3.64	-0.54	-0.51	-0.77	-1.37
	b2	-0.85	-2.96	-0.49	-0.50	-0.78	-1.02
	b3	-0.70	-2.19	-0.41	-0.49	-0.82	-0.63
	b4	-0.59	-1.55	-0.33	-0.49	-0.86	-0.28
	b5	-0.52	-1.12	-0.25	-0.48	-0.88	-0.03
	b6	-0.48	-0.91	-0.18	-0.45	-0.89	-0.08
Water level	c0_areal	-0.52	-0.42	-6.83	-1.38	-6.76	-1.57
	c1_areal	-0.89	-0.14				
	c0_shear	-0.75	0.78	-3.14	0.13	2.23	0.89

A. STRAIN RESPONSE TO EARTH TIDES

In Table 2, the areal tidal coefficients are generally distributed from 1 to 3. We further evaluated the tidal factors of the M_2 component through harmonic analysis using T-Tide MATLAB package, with the tidal factors from 0.8 to 1.2 [54], which agree with the values of the tidal response coefficients computed using the Kalman filter. The coefficients are slightly larger because the coefficients of the state-space model are correspond to all the components of the earth tides. Tidal loading in shear strain is more evident because the subtraction of the strain can eliminate some environmental effects such as air pressure. The shear tidal coefficients are larger than the areal tidal coefficients ranging from 2 to 5, which agree with the behaviour of the steel cylinder, i.e., changing its area is more difficult than changing its shape. Therefore, the model is capable of removing the tidal response in the strainmeters.

B. STRAIN RESPONSE TO AIR PRESSURE

Barometric interference is negatively correlated with strain. We estimated the coefficients of the air pressure response, b0, b1, b2, $\cdots$, for six stations listed in Table 2. As the fitting order of the model of each station is different, we show only the first six coefficients of the air pressure response. In Table 2, $b0$, as a timely load response, is the largest value in the most case, which is within the range of $-1\sim$-3nε/hPa. According to Hooke's law, the YRY4 strainmeters measure the horizontal two-dimensional strain, where the horizontal stresses are assumed as follows:

$$\varepsilon_1 + \varepsilon_2 = \frac{1}{E}(\sigma_1 + \sigma_2 - \mu(\sigma_1 + \sigma_2)), \tag{9}$$

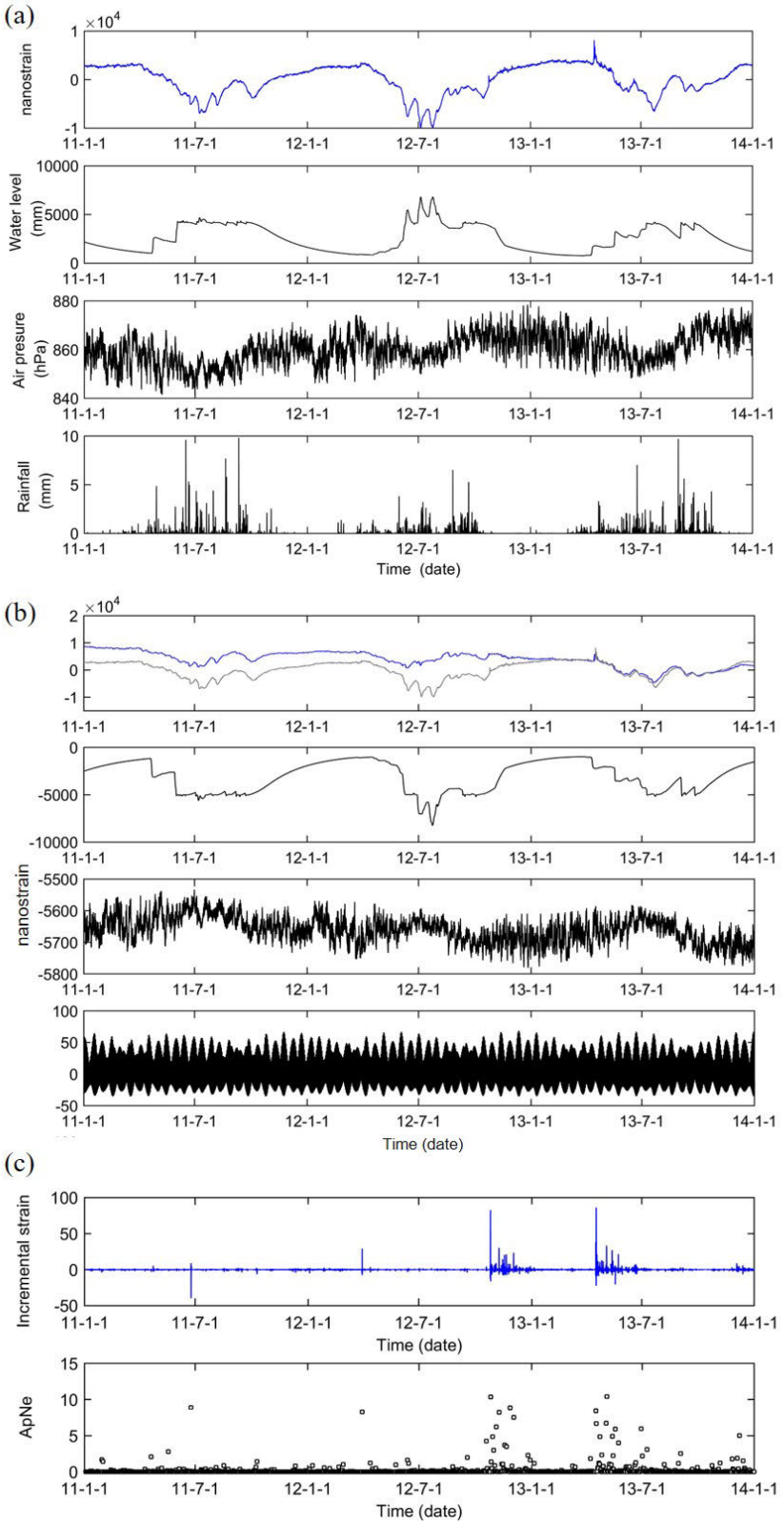

FIGURE 2. (a) Hourly raw areal strain (blue), water level, air pressure, and rainfall data at the GZ station. (b) The first panel is the corrected strain (blue) and the raw strain (grey); other panels show the induced strain of the water level, air pressure, and earth tides. (c) The increments of the corrected strain (blue) and the daily approximate negentropy (ApNe).

where ε_1 and ε_2 are the horizontal strain values, σ_1 and σ_2 are the corresponding stresses, and E and μ are the Young's modulus and the Poisson's ratio, respectively. Assuming $\mu = 0.25$ and $E = 0.5 \times 10^9$hPa, the amplitude of the compressive horizontal strain is -1.50 nε/hPa, which is comparable to the observed values.

However, Hooke's law is a simple model of elastic mechanics. Based on the velocity of the pressure disturbance and the depth of the crust, the air pressure response changes over time. In the state-space model, the response to a step change in air pressure can be expressed as the cumulative sum of the air pressure coefficients. Figure 3 shows the estimated response to a step change in air pressure obtained from all air pressure coefficients. In general, the response gradually reaches its limiting value, i.e., -4 to -17 nε/hPa, over a period of approximately 5∼13 h. This time range is related to the skin factor and the transmissivity of the borehole [55].

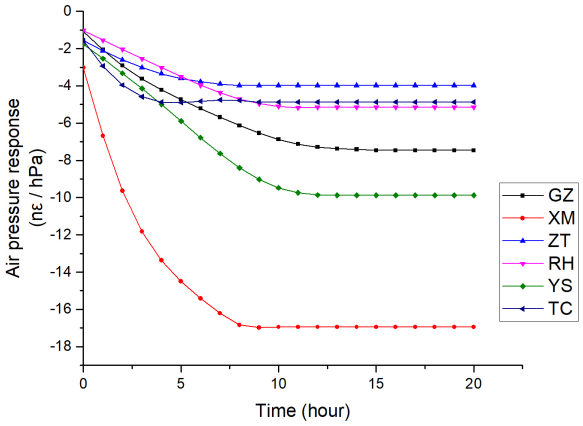

FIGURE 3. Response to a step change in air pressure with the air pressure coefficients.

Theoretical calculations of the effect that the pressure field on crustal loading show the relationship between the air pressure coefficient of the areal strain, which changes with the crustal depth, and the pressure disturbance period [32]:

$$\varepsilon = \frac{3}{2}\frac{1}{2E}e^{-\frac{\pi z}{\tau v}}((3.3\mu - 3.7) + \frac{4}{5}\frac{\pi z}{\tau v}(1-\mu)) \qquad (10)$$

where E and μ are the Young's modulus and the Poisson's ratio, respectively, z is the installation depth of the borehole strainmeter, and τ is the period of a single air pressure wavelength, and v is the velocity of the pressure disturbance. Assuming that $\mu = 0.25$ and $E = 0.5 \times 10^9$hPa, the average disturbance velocity of the air pressure change is 4.5 m/s. At a depth of 40 m in the crust hole, the pressure coefficient is stable at approximately -4.27 nε/hPa. When there is a relatively loose layer with small E values (e.g., 0.2×10^9hPa) of a strainmeter,such as the XM and YS stations, the pressure coefficient exceeds -10 nε/hPa. The porosity of the rock also yields a discrepancy in the barometric coefficient. Previous studies have used linear regression methods to obtain the strainmeter response to air pressure [56]. Such estimates of the air pressure coefficients are approximately 0 to -9nε/hPa at these six stations. Therefore, we consider that the air pressure coefficients are comparable to the expected values.

C. STRAIN RESPONSE TO WATER LEVEL

Rainfall, snowmelt, pumping, and changes in the water level of a river or a reservoir cause changes in the loading around a borehole. The strain and water level observations typically exhibit a negative correlation, i.e., when the water level rises (loading increases), the strain curve decreases (compression). Estimates of the induced areal strain due to the changes in groundwater levels are within the range of -0.5 to -7.0 nε/mm. We computed the theoretical horizontal strain per meter of water level change (equivalent to 10^4 Pa) using Equation 9. The groundwater response to the strain is 0.15 nε/mm, consistent with the observed values of -0.5 to -7.0 nε/mm considering the layers with smaller G values or larger porosities. Liu *et al.* [56] linearly added the influence of the water level to the Nakai model to evaluate the fitting coefficients via the least square method. The obtained water level efficiencies were also in the range of 0 to -10 nε/mm.

The absolute amplitudes of the coefficients of the level of the shear and theoretical strains induced by the changes in groundwater levels have the same order of magnitude; however, there are positive and negative coefficients. Local conditions may be anisotropic owing to the influence of the surrounding broken zones or reservoirs, changing the linear strains of the four components. If the water level is positively related to one of the component strains, it may also be positively related to the shear strain. The situation for each observation point requires further specific analysis. The hydraulic environment adjacent to the borehole is also important and thus should be considered when selecting the installation location of strainmeters.

D. STRAIN RESPONSE TO RAINFALL

In general, rainfall infiltration increases the water level in the borehole, which is affected by compressive stress, and decreases the strain. The rainfall effect is usually expressed by an autoregressive-moving-average model with the exogenous input model that considers the immediate and delayed effects of rainfall [34]. However, rainfall-induced strain is the most complicated one of all the environment-induced strains. First, not every rainfall event can be described by using a mathematical model; pore saturation is different for heavy and light rainfall events. Second, there may be additional strain from fluid pressure changes that take place due to rainfall infiltration. Third, if there are rivers and reservoirs around a borehole, rainfall will have a magnifying effect on the strain.

If the model results have large misfits, the error in the corrected strains will increase. Therefore, we tend to analyse the rainfall effect on strain case by case at present. We performed a simple linear regression with observed strain values and cumulative rainfall (without trends). The raw areal strain, water-level-induced strain calculated by the Kalman filter

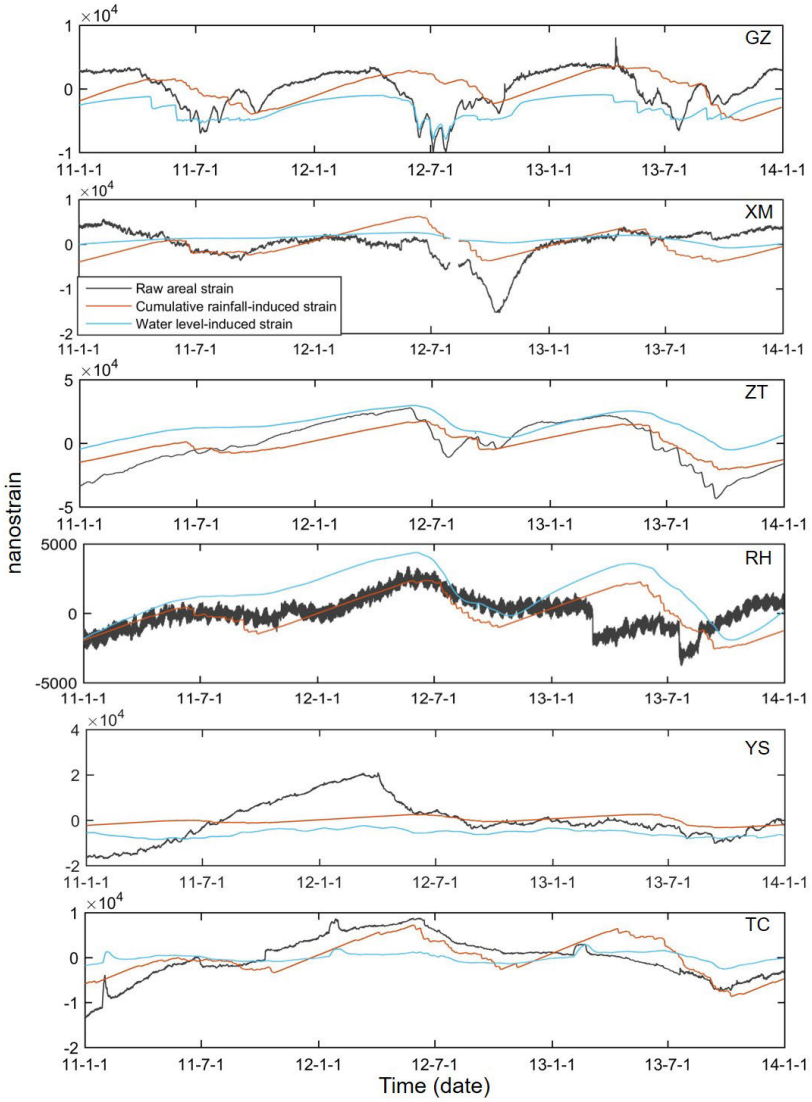

FIGURE 4. Raw areal strain, water-level-induced strain, and cumulative rainfall-induced strain at six stations.

method, and cumulative rainfall-induced strain are shown in Fig. 4. These strain values showed a strong correlation at the GZ, XM, ZT, RH, and TC stations. The response to rainfall ranged from -1 to -6 nε/mm, consistent with the response to the water level (-0.5 to -7 nε/mm) and air pressure (-4 to -17 nε/hPa).

V. EXTRACTING PRE-EARTHQUAKE STRAIN ANOMALIES FOR THE LUSHAN EARTHQUAKE

A. ApNe ANOMALIES OF CORRECTED STRAIN DATA

The interior physics of the earthquake process is complex. For example, there may be certain precursors that originate from underground activities, which lead to larger earthquakes. However, there may also be certain precursors that do not create anomalies. Thus, spatiotemporal clustering is considered to represent the most striking departure from randomness for the large earthquake occurrence process [57]. For clustered accumulation anomalies, the sigmoid function was applied to describe such changes. The sigmoid function is characterised by two power law behaviours with opposite concavities before and after a centre point, which can be expressed as follows:

$$y = A2 + \frac{(A1 - A2)}{(1 + e^{\frac{x - x0}{dx}})}, \tag{11}$$

where $A1$, $A2$, $x0$, and dx are the asymptotic lower limit, asymptotic upper limit, inflection point, and time constant, respectively. These parameters are widely used to describe seismic anomalies [58]. If the earthquake events and anomalies have no correlation, the accumulation for random anomalies should increase linearly. In contrast, if the slope of the accumulation curve increases prior to an earthquake, this indicates a possible relationship between the anomalies and

external strain sources, especially when local environmental responses from the raw strain are eliminated via the state-space model.

We computed the daily ApNe value of the corrected strain from 1 January 2011 to 1 January 2014 to illustrate the underground instability of the southwestern endpoint of the Longmenshan fault zone. We assumed that an anomaly exists if the ApNe value exceeds the mean plus two standard deviations. In that case, we applied one count for the corresponding day, then summed the counts over time. Figure 5 shows the cumulative ApNe anomaly results for areal strain at six stations.

In Fig. 5(a), the ApNe anomalies at the GZ, XM, and RH stations before the Lushan earthquake are not as random as those in 2011. The first acceleration of the ApNe anomaly accumulation occurred approximately six to four months prior to the earthquake, showing an abrupt acceleration followed by moderate acceleration, which indicates that non-Gaussian changes in the borehole strain data began to appear. This implies that strain anomalies changed from unorganised to organised. Based on Prigogine and Stengers [46], the entropy can decrease depending on the energy flux ratio in an open system. Accordingly, the increase in ApNe anomalies may reflect the fact that the influence of external forces stimulates energy accumulation in the formation of a seismic source area [59]. In addition, from the day of the earthquake until two months after the earthquake, the second cluster of anomalies briefly increased and recovered to a stable state, with a downward concavity, illustrating the deceleration and recovery of anomaly accumulation. Moreover, the two clusters of anomalies are consistent with the findings of previous studies on borehole strain associated with the 2013 Lushan earthquake [25], [42].

However, the accumulations of the ApNe anomalies at the distant YS, RH, and TC stations are linear (Fig. 5(b)) and can be regarded as random anomalies, indicating that these stations may not have detected the pre-earthquake anomalies. They are far from the Southern end of the Lushan earthquake fault such that no observations of anomalous changes would be reasonable.

To further investigate the relationship of the occurrence of these anomalies with the Lushan earthquake, we statistically analysed the acceleration rate of the ApNe anomalies from each station before the earthquake. We selected the same period with anomaly accumulation in the last three months of 2012 at six stations and used their slopes to represent the acceleration rate. For comparison, we normalised the number of anomalies involved in the linear fit. As the epicentral distance increased, the acceleration rate decreased exponentially. In Fig. 5(c), the anomaly acceleration rate and corresponding epicentral distance are strongly correlated and subject to a linear logarithmic relationship: $AR_a = -0.0063 \log(R) + 0.019$, with a goodness-of-fit of 0.65. Here, AR_a, and R are the acceleration rate for areal strain, and epicentral distance, respectively. We performed the same

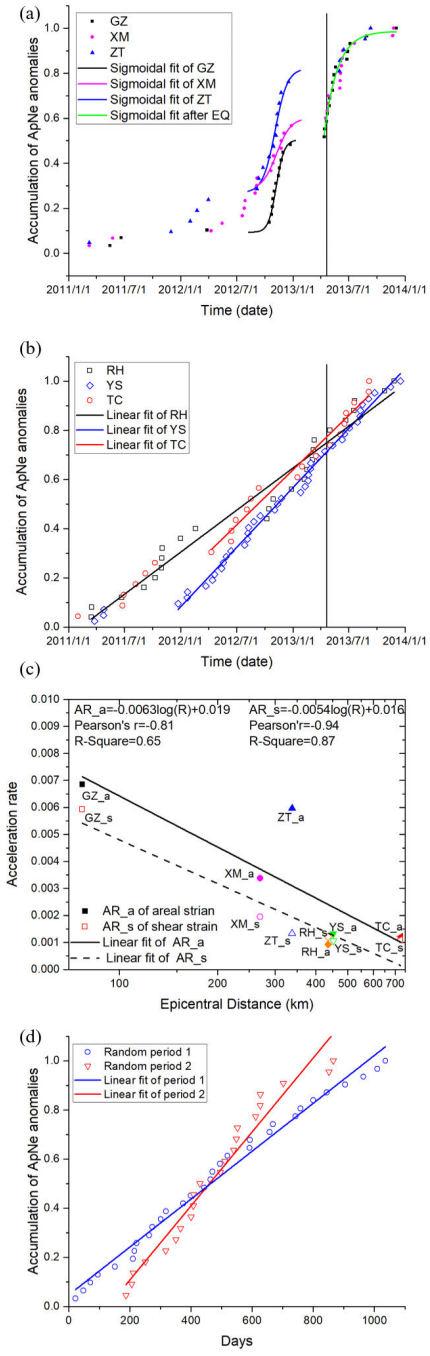

FIGURE 5. (a) Accumulation of ApNe anomalies at the GZ, XM, and ZT stations. The solid dots are the cumulative ApNe anomaly counts from 2011-2014. The black, pink, and blue lines are the sigmoidal fits at the GZ, XM, and ZT stations. The green line is the sigmoidal fit after the earthquake at the GZ station. The vertical red line is the day of the 2013 Lushan earthquake. (b) The accumulation of negentropy anomalies at the RH, YS, and TC stations. The black, pink, and blue lines are their linear fits. (c) Relationship between the epicentral distance and acceleration rate both for areal and shear strain values at each station. Solid dots represent the acceleration rate of the areal strain, AR_a, and hollow dots correspond to the shear strain, AR_s. The black lines are their linear fits at logarithmic epicentral distances. (d) The accumulation of ApNe anomalies for two random periods. Period 1 is from 1 January 2009 to 1 January 2012. Period 2 is from 1 July 2014 to 1 July 2016.

process for the borehole shear strain, i.e., extracting the ApNe anomalies, followed by fitting their anomaly accumulations. The results for shear strain, AR_s, were similar to the areal strain results (Fig. 5(c)). The deviation at the ZT station was large because it was surrounded by earthquake-prone areas during that period, and the shear strain may have weakened these changes. Generally speaking, as the epicentral distance increases, the acceleration rate becomes less significant, indicating that the ApNe anomalies are more sensitive near the 2013 Lushan earthquake epicentre. In other words, the ApNe anomalies from the borehole strain data depend on the epicentre of the Lushan earthquake.

B. COMPARISON WITH RANDOM PERIODS

To improve the statistical significance of the anomalies, we expanded the dataset and compared two random periods. Period 1 is from 1 January 2009 to 1 January 2012, and period 2 is from 1 July 2014 to 1 July 2016. There were no strong earthquakes in the selected periods, and the data quality was high. We performed ApNe analysis on these two random periods and compared them with the 2013 Lushan earthquake (Fig. 5(d)). The accumulation of the ApNe anomalies in the random periods are characterised by a statistically significant linear increase. These two periods include five years' worth of data, which implies that linear accumulation can be regarded as a normal-state background of ApNe accumulation. However, during the Lushan earthquake period, as the earthquake approached (October to December 2012), the number of ApNe anomalies increased rapidly and recovered after the earthquake. This comparison indicates that the extracted ApNe anomalies are different from the normal-state background.

C. DAILY VARIATIONS OF B VALUES

Crustal deformation is a highly complicated process; an integrated analysis and interpretation of other geophysical observations can improve the understanding of the earthquake process. From the elastic deformation stage to the unstable stage of rock fractures, the number of small earthquakes increases [60], which explains the earthquake sequences before a strong earthquake occurs [61]. Based on an analysis of the earthquake catalogue from 1 January 2011 to 1 January 2014, we further investigated the b value prior to the Lushan earthquake. Figure 6 shows the temporal variations in the b value derived by a moving window of 500 samples, with a 20-sample step size. The b value started to increase in 2011 and gradually reached its maximum value in 2012. After September 2012, there was a rapid decline, which was sustained until 2013. At the beginning of 2013, the b value rebounded slightly until the Lushan earthquake. After the earthquake, the b value recovered.

The decreasing trend of the b value and ApNe anomalies for the borehole strain indicate that, after September 2012, the strain accumulation likely experienced abnormal changes along the southern end of the Longmenshan fault zone.

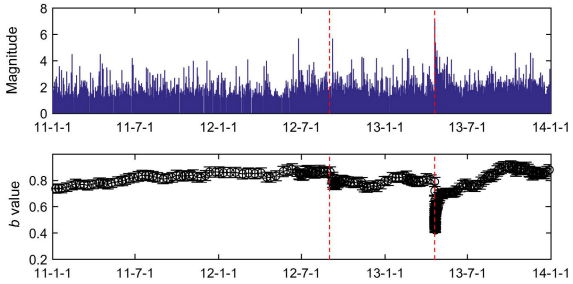

FIGURE 6. (a) Temporal distribution of earthquakes ($Ms \geq 1$) from 2011 to 2014. (b) Temporal variations in the b values. The black line shows the temporal variations in b values with their error bars in 2011-2014 for a window length of N = 500 and step = 20. The vertical red lines are the time labels for September 2012 and earthquake day.

The lower b value after the earthquake also corresponds to the ApNe anomalies after the earthquake.

At the initial stage of the earthquake, the entire fault slides stably under the tectonic stress, where the accumulation of ApNe anomalies increases linearly. With the increase in the tectonic stress, local crustal movements gradually change from a linear stage to a nonlinear stage. During this period, as the stress continues to accumulate, small local cracks and slips at different scales occur. A locked area forms when frictional resistance along the fault is greater than the shear stress across the fault. Under tectonic stress, the sliding zones along the fault still maintain relative movement with respect to each other, resulting in the continual accumulation of elastic energy in the locked area. In this period, the ApNe anomalies increase quickly while the b value is low. However, when this process develops to a certain stage, the deformation is dominated by a release and part of the locked areas are unlocked to become the slip areas, with an expansion of the sliding areas. In the remaining locked areas, especially near the new breakpoint, the further concentration and redistribution of stress result in an increasingly high stress concentration degree [24]. Certain weak parts are destroyed, resulting in stress release, which corresponds to a slight rebound in the b value before the earthquake. At this stage, the fault zone is stable and shows 'quiescence' with significantly weakened deformation. Thus, strain data record no ApNe anomalies. When the locked region with an increasing stress concentration cannot support the accumulated strong shear stress, the entire locked region instantly destabilizes, promoting the occurrence of the earthquake. The in situ stress measurement results in the southwestern area of the Longmenshan fault zone also indicate that the maximum horizontal principal stress in this area has reached a critical low limit for the fault's active stress after the 2008 Wenchuan earthquake, and fault activity has entered a critical state [62]. The Lushan earthquake occurred due to the fault displacement caused by the shear stress along the seismogenic fault plane that exceeded the threshold [63]. Besides this, in the locked region, there is a significant end effect on the stress distribution [64] such that the southwestern end of the Longmenshan fault zone is a potential region where the anomaly can occur.

Studies that analysed the GPS data between 2009 and 2011 have shown that the southwestern endpoint of the Longmenshan fault zone, before the Lushan earthquake occurred, was locked [22]. The investigations of the changes in the GNSS baseline length showed that the trends in the GNSS baseline had an abnormal deviation for several months before the Lushan earthquake [24]. The maximal shear strain and the first shear strain showed a significant pre-seismic locking process that occurred from September to December 2012 (Fig. 9 in [24]), which is also consistent with our results.

The complexity of crustal deformation, the uncertainty of the seismogenic mechanism, and the uneven distribution of the fault and cross-fault measurement sites make the examination of the pre-earthquake process challenging. Although these results may objectively reflect the seismogenic process associated with the 2013 Lushan earthquake, further exploration of the mechanism for these anomalies and improved statistics are required to fully understand the dynamic background of the earthquake.

VI. CONCLUSION

To verify the existence of the strain precursors preceding the 2013 Lushan earthquake, we applied an anomaly detection method based on a space-state model and ApNe analysis to the borehole strain data from 2011−2014 along the southwestern end of the Longmenshan fault zone. First, we ruled out several local factors that may have affected the strain. As for the environmental disturbances, we constructed a state-space model that uses air pressure, earth tides, and water level data based on the observations recorded using YRY-4 borehole strainmeters. The obtained tidal, air pressure, and water level efficiencies were from 1 to 5, from −4 to −17 nε/hPa, and from −0.5 to −7.0 nε/mm, respectively. We then performed an ApNe analysis of the corrected data from six stations. The temporal results at the GZ, XM, and ZT stations for the ApNe anomaly accumulation were almost simultaneously accelerated four to six months prior to the earthquake. Further investigations of the anomaly accumulation rate showed that the extracted ApNe anomalies depended on the epicentral distance. Comparison analysis with the ApNe anomaly accumulation in other random time periods further demonstrates the significance of the extracted anomalies. Moreover, our results were consistent with the b values and GNSS geodetic data. Therefore, we conclude that the state-space model can effectively decompose the strain data and ApNe analysis has the potential to enhance the understanding of the earthquake generation process. Future studies should focus on strain precursor mechanisms and statistical analyses of higher-dimensional observations.

APPENDIX A
STATE-SPACE ANALYSIS OF BOREHOLE STRAIN BY KALMAN FILTER

For the clean strain, S_n^{ca} and S_n^{cs}, that cannot be observed or measured in state-space models, the Kalman filter was applied to the optimal estimates of the state vector by iterating the covariance matrix [65]. We used the state-space model of the areal strain as an example. A state vector, z_n, are assumed that it can fully describe the system of Equation 4 at time n.

$$z_n = (S_n^{ca}, a_0, \ldots, a_m, b_0, \ldots, b_l, c_0, \ldots, c_k)^{\mathrm{T}}. \quad (12)$$

Here, S_n^{ca} is the corrected areal strain, which is considered the tectonic-origin strain. The state vector z_n depends upon its value at $n-1$, which can be written as a transition equation:

$$\begin{aligned} z_n &= Bz_{n-1} + v_n, \\ v_n &\sim N(0, Q), \quad n = 1, 2, \ldots, N \end{aligned} \quad (13)$$

where the process noise, v_n, is the Gaussian white noise with a process noise covariance of Q. B as the state-transition matrix, can be expressed as follows:

$$B = \begin{pmatrix} 1 & & & \\ & I_{m+1} & & \\ & & I_{l+1} & \\ & & & I_{k+1} \end{pmatrix}, \quad (14)$$

where I refers to the identity matrix. The borehole strain at time n can be estimated by the state vector of the air pressure, solid tide, and water level according to a measurement equation:

$$S_n^a = G_n z_n + \varepsilon_n, \quad (15)$$

which describes the relationship between the observed strain, S_n^a, and unobserved state, z_n. The measurement matrix, G_n, is expressed as follows:

$$G_n = (1, p_n, \ldots, p_{n-l}, e_n, \ldots, e_{n-m}, w_n, \ldots, w_{n-k}). \quad (16)$$

The Kalman filter is a recursive procedure that corrects the estimation by continuously predicting and updating one point at a time. Here, $z_{n|n-1}$ and $F_{n|n-1}$ represent the estimated state and the variance-covariance matrix at time n based on observations for times $n-1$, as follows:

$$z_{n|n-1} = Bz_{n-1|n-1}, \quad (17)$$

where

$$F_{n|n-1} = BF_{n-1|n-1}B^{\mathrm{T}} + Q. \quad (18)$$

Having observed the data for S_n^{ca}, we can update the predictions, i.e., $z_{n|n-1}$ and $F_{n|n-1}$, according to the Kalman filter (1960).

However, we note that the covariance of the measurement noise, R, in a conventional Kalman filter is constant. Based on the state-space equation, external environmental factors, such as the air pressure and water level, not only effect the measurement strain, but also change the measurement noise associated with the observed strain. Therefore, the measurement noise, R, can be improved to dynamic noise, R_n. For dynamic noise estimation, an adaptive Kalman filter is widely used [66]. We introduced the amnestic factor, d_n, and forgetting factor, b, which range from 0 to 1, to estimate the optimal state, i.e., $z_{n|n}$. Here, d_n is regarded as a decreasing

weight function. By adjusting b, R_n is corrected to obtain the dynamic covariance estimation with the largest weight on the current observation value. The implementation steps of the Kalman filter adapted to measurement noise are as follows:

$$K_n = F_{n|n-1}G_n^{\mathrm{T}}(G_nF_{n|n-1}G_n^{\mathrm{T}} + R_n)^{-1}, \quad (19)$$
$$V_n = S_n^a - G_nz_{n|n-1}, \quad (20)$$
$$z_{n|n} = z_{n|n-1} + K_nV_n, \quad (21)$$
$$F_{n|n} = (I - K_n)F_{n|n-1}, \quad (22)$$
$$R_n = (1 - d_n)R_{n|n-1} + d_n(V_nV_n^{\mathrm{T}}). \quad (23)$$

Here,

$$d_n = (1 - b)/(1 - b^n). \quad (24)$$

where K_n is the filter gain, V_n is the remainder vector, $F_{n|n}$ is the covariance matrix of the state estimation, and $F_{n|n-1}$ is the one-step estimation variance matrix. The best orders, i.e., l, m, and k, for the model were determined by minimizing the Akaike's Information Criterion (AIC) [67], as the Kalman filter allows the construction of the likelihood function associated with the state-space model [68].

APPENDIX B
APPROXIMATE NEGENTROPY ANALYSIS OF CORRECTED STRAIN

As the Gaussian random variable is considered to have the largest entropy and the highest randomness of all other random variables with equal variance [69], the entropy-based negentropy is used as a statistically justified measure of non-randomness [70]. The definition of negentropy Ne is as follows:

$$Ne(Y) = H(Y_{guass}) - H(Y), \quad (25)$$

where Y_{gauss} is a Gaussian random strain, with the same mean and covariance matrix as the incremental strain y. The entropy H of a random variable, $Y = \{y_1, y_2, \ldots, y_i, \ldots\}$, can be defined as follows:

$$H(Y) = -\sum_i P(y_i)\log P(y_i), \quad (26)$$

where P is the probability density function (PDF). Previous research derived that higher order statistics (HOS) can be used to approximate one-dimensional negentropy [71]:

$$ApNe(Y) \approx \frac{1}{12}skewness^2(Y) + \frac{1}{48}kurtosis^2(Y). \quad (27)$$

The *skewness* and *kurtosis* are the third- and fourth-order statistics, respectively, which are defined as

$$skewness(Y) = \frac{\mu_3}{\sigma^3} = \frac{E[(Y-\mu)^3]}{E[(Y-\mu)^2]^{3/2}} \quad (28)$$

and

$$kurtosis(Y) = \frac{\mu_4}{\sigma^4} = \frac{E[(Y-\mu)^4]}{E[(Y-\mu)^2]^2} - 3, \quad (29)$$

where μ is the mean of Y and σ is the standard deviation of Y. Skewness is a measure of asymmetry in a PDF. A symmetric distribution has zero skewness. Kurtosis is a measure of tail heaviness in a PDF. Distributions that are more outlier-prone than a normal distribution have kurtosis values greater than zero. Based on the definitions above, skewness and kurtosis can be regarded as the normalization of third- and fourth-order moments.

ACKNOWLEDGMENT

The borehole strain data can be acquired at the National Earthquake Precursor Network Centre (http://qzweb.seis.ac.cn/twzx, last access: 09 October 2017). The authors would like to thank Wang X. Y., Yang D. H., and Yu H. C. from the China Earthquake Administration for providing access to the website and downloading the strain data. The authors also thank the China Earthquake Network for earthquake catalogue data (http://data.earthquake.cn/, last access: 15 March 2020). Moreover, the authors are grateful to Prof. Qiu Z. H., Prof. Niu A. F., and Liu Q. for their guidance and helpful suggestions.

REFERENCES

[1] A. McGarr, I. S. Sacks, A. T. Linde, S. M. Spottiswoode, and R. W. E. Green, "Coseismic and other short-term strain changes recorded with Sacks-Evertson strainmeters in a deep mine, South Africa," *Geophys. J. Roy. Astronomical Soc.*, vol. 70, no. 3, pp. 717–740, Sep. 1982.
[2] Z. Zhang, S. Ying, and Y. Shen, "Crustal deformation before strong earthquakes and utility of earthquake prediction by geodetic measurements: Extended abstract," *J. Phys. Earth*, vol. 34, no. 2, pp. S111–S127, 1986.
[3] H. Hirose, "Tilt records prior to the 2011 off the pacific coast of Tohoku earthquake," *Earth, Planets Space*, vol. 63, no. 7, pp. 655–658, Jul. 2011.
[4] Y. Asai, M. Okubo, H. Ishii, H. Aoki, T. Yamauchi, Y. Kitagawa, and N. Koizumi, "Co-seismic strain-steps associated with the 2004 off the Kii peninsula earthquakes-observed with Ishii-type borehole strainmeters and quartz-tube extensometers," *Earth, Planets Space*, vol. 57, no. 4, pp. 309–314, Apr. 2005.
[5] T. Parsons, C. Ji, and E. Kirby, "Stress changes from the 2008 Wenchuan earthquake and increased hazard in the Sichuan basin," *Nature*, vol. 454, no. 7203, pp. 509–510, Jul. 2008.
[6] M. Wei, D. Sandwell, and B. Smith-Konter, "Optimal combination of InSAR and GPS for measuring interseismic crustal deformation," *Adv. Space Res.*, vol. 46, no. 2, pp. 236–249, Jul. 2010.
[7] C.-H. Chen, T.-K. Yeh, J.-Y. Liu, C.-H. Wang, S. Wen, H.-Y. Yen, and S.-H. Chang, "Surface deformation and seismic rebound: Implications and applications," *Surv. Geophys.*, vol. 32, no. 3, p. 291, 2011.
[8] T. Wang, J. Zhuang, T. Kato, and M. Bebbington, "Assessing the potential improvement in short-term earthquake forecasts from incorporation of GPS data," *Geophys. Res. Lett.*, vol. 40, no. 11, pp. 2631–2635, Jun. 2013.
[9] Z. Wang, J. Su, C. Liu, and X. Cai, "New insights into the generation of the 2013 Lushan earthquake (Ms7.0), China," *J. Geophys. Res., Solid Earth*, vol. 120, no. 5, pp. 3507–3526, May 2015.
[10] M. Moro, M. Saroli, S. Stramondo, C. Bignami, M. Albano, E. Falcucci, S. Gori, C. Doglioni, M. Polcari, M. Tallini, L. Macerola, F. Novali, M. Costantini, F. Malvarosa, and U. Wegmüller, "New insights into earthquake precursors from InSAR," *Sci. Rep.*, vol. 7, no. 1, p. 12035, Dec. 2017.
[11] M. T. Gladwin, "High-precision multicomponent borehole deformation monitoring," *Rev. Sci. Instrum.*, vol. 55, no. 12, pp. 2011–2016, Dec. 1984.
[12] Z.-H. Qiu and Y.-L. Shi, "Developments of borehole strain observation outside China," *Acta Seismologica Sinica*, vol. 17, no. 1, pp. 172–178, Nov. 2004.
[13] M. Johnston, A. Linde, and D. Agnew, "Continuous borehole strain in the San Andreas fault zone before, during, and after the 28 June 1992, M_w 7.3 Landers, California, earthquake," *Bull. Seismol. Soc. Amer.*, vol. 84, no. 3, pp. 799–805, 1994.
[14] A. T. Linde, M. T. Gladwin, M. J. S. Johnston, R. L. Gwyther, and R. G. Bilham, "A slow earthquake sequence on the San Andreas fault," *Nature*, vol. 383, no. 6595, pp. 65–68, Sep. 1996.

[15] Z. Qiu, B. Zhang, S. Chi, L. Tang, and M. Song, "Abnormal strain changes observed at Guza before the Wenchuan earthquake," *Sci. China Earth Sci.*, vol. 54, no. 2, pp. 233–240, Feb. 2011.
[16] L. Qi and Z. Jing, "Application of S transform in analysis of strain changes before and after Wenchuan earthquake," (in Chinese), *J. Geodesy Geodynamics*, vol. 31, no. 4, pp. 6–9, 2011.
[17] I. S. Sacks, A. T. Linde, S. Suyehiro, and J. A. Snoke, "Slow earthquakes and stress redistribution," *Nature*, vol. 275, no. 5681, pp. 599–602, 1978.
[18] I. S. Sacks, A. T. Linde, J. A. Snoke, and S. Suyehiro, "A slow earthquake sequence following the Izu-Oshima earthquake of 1978," *Earthq. Predict., Int. Rev.*, vol. 4, pp. 617–628, Jan. 1981.
[19] Z. H. Qiu and Y.-L. Shi, "Observations of remote coseismic stress step-changes," *Sci. China Ser. D, Earth Sci.*, vol. 46, no. 2, pp. 75–81, 2003.
[20] Z. Qiu, S. Chi, Z. Wang, S. Carpenter, L. Tang, Y. Guo, and G. Yang, "The strain seismograms of P- and S-waves of a local event recorded by four-gauge borehole strainmeter," *Earthq. Sci.*, vol. 28, no. 3, pp. 209–214, Jun. 2015.
[21] E. Sturkell, K. Ágústsson, A. T. Linde, S. I. Sacks, P. Einarsson, F. Sigmundsson, H. Geirsson, R. Pedersen, P. C. LaFemina, and H. Ólafsson, "New insights into volcanic activity from strain and other deformation data for the Hekla 2000 eruption," *J. Volcanol. Geothermal Res.*, vol. 256, pp. 78–86, Apr. 2013.
[22] Y. Wu, Z. Jiang, and M. Wang, "Preliminary results of the co-seismic displacement and pre-seismic strain accumulation of the Lushan Ms7.0 earthquake reflected by the GPS surveying," *Chin. Sci. Bull.*, vol. 58, no. 20, pp. 1910–1916, 2013.
[23] X. Kong, N. Li, L. Lin, P. Xiong, and J. Qi, "Relationship of stress changes and anomalies in OLR data of the Wenchuan and Lushan earthquakes," *IEEE J. Sel. Topics Appl. Earth Observ. Remote Sens.*, vol. 11, no. 8, pp. 2966–2976, Aug. 2018.
[24] K. Xu, W. Gan, and J. Wu, "Pre-seismic deformation detected from regional GNSS observation network: A case study of the 2013 Lushan, Eastern Tibetan Plateau (China), Ms 7.0 earthquake," *J. Asian Earth Sci.*, vol. 180, Aug. 2019, Art. no. 103859.
[25] S. Chi, Q. Liu, Y. Chi, T. Deng, C. Liao, G. Yang, G. Zhang, and J. Chen, "Borehole strain anomalies before the 20 April 2013 Lushan Ms7.0 earthquake," (in Chinese), *Acta Seismol Sin*, vol. 35, no. 3, pp. 296–303, 2013.
[26] L. Yi, Z. Jing, C. Sunliang, and Y. Wei, "Time-frequency characteristics of four-component borehole strain at Guzan station before and after 2013 Lushan Ms7.0 earthquake," (in Chinese), *Acta Seismol. Sinica*, vol. 36, no. 5, pp. 770–779, 2014.
[27] K. Zhu, C. Chi, Z. Yu, W. Zhang, M. Fan, K. Li, and Q. Zhang, "Extracting borehole strain precursors associated with the Lushan earthquake through principal component analysis," *Ann. Geophys.*, vol. 61, pp. 1593–5213, Sep. 2018.
[28] Y.-J. Hsu, Y.-S. Chang, C.-C. Liu, H.-M. Lee, A. T. Linde, S. I. Sacks, G. Kitagawa, and Y.-G. Chen, "Revisiting borehole strain, typhoons, and slow earthquakes using quantitative estimates of precipitation-induced strain changes," *J. Geophys. Res., Solid Earth*, vol. 120, no. 6, pp. 4556–4571, Jun. 2015.
[29] Z. Lu, H. Yi, and L. Wen, "Loading-induced Earth's stress change over time," *J. Geophys. Res., Solid Earth*, vol. 123, no. 5, pp. 4285–4306, May 2018.
[30] C. Chi, K. Zhu, Z. Yu, M. Fan, K. Li, and H. Sun, "Detecting earthquake-related borehole strain data anomalies with variational mode decomposition and principal component analysis: A case study of the Wenchuan earthquake," *IEEE Access*, vol. 7, pp. 157997–158006, 2019.
[31] X. Zhang, "A necessity of higt-precise assistance measurement for atmospheric pressure and correction of atmosphric pressure effect in tidal observation," *Crustal Deformation Earthq.*, vol. 4, no. 4, pp. 273–280, 1987.
[32] L. S. Zhou, Z. H. Qiu, and L. Tang, "The response of crustal strain field to short-period atmospheric pressure variation," (in Chinese), *Prog. Geophys.*, vol. 23, no. 6, pp. 1717–1726, Dec. 2008.
[33] L. Zhang, "Influences of rainfall on body strain," (in Chinese), *Crustal Deformation Earthq.*, vol. 3, no. 15, pp. 78–83, 1995.
[34] N. Matsumoto, G. Kitagawa, and E. A. Roeloffs, "Hydrological response to earthquakes in the Haibara well, central Japan–I. Groundwater level changes revealed using state space decomposition of atmospheric pressure, rainfall and tidal responses," *Geophys. J. Int.*, vol. 155, no. 3, pp. 885–898, Dec. 2003.
[35] S. Chi, "China's component borehole strainmeter network," *Earthq. Sci.*, vol. 22, no. 6, pp. 579–587, Dec. 2009.
[36] E. Roeloffs, "Tidal calibration of plate boundary observatory borehole strainmeters: Roles of vertical and shear coupling," *J. Geophys. Res.*, vol. 115, no. 6, pp. 1–25, 2010.
[37] K. Eftaxias, Y. Contoyiannis, G. Balasis, K. Karamanos, J. Kopanas, G. Antonopoulos, G. Koulouras, and C. Nomicos, "Evidence of fractional-Brownian-motion-type asperity model for earthquake generation in candidate pre-seismic electromagnetic emissions," *Natural Hazards Earth Syst. Sci.*, vol. 8, no. 4, pp. 657–669, Jul. 2008.
[38] P. Manshour, S. Saberi, M. Sahimi, J. Peinke, A. F. Pacheco, and M. R. R. Tabar, "Turbulencelike behavior of seismic time series," *Phys. Rev. Lett.*, vol. 102, no. 1, Jan. 2009, Art. no. 014101.
[39] X. Sun, G. Wang, and Y. Rui, "Extracting high-frequency anomaly information from fluid observational data: A case study of the Wenchuan Ms 8.0 earthquake of 2008," (in Chinese), *Chin. J. Geophys.*, vol. 59, no. 5, pp. 1673–1684, 2016.
[40] H.-J. Chen and C.-C. Chen, "Testing the correlations between anomalies of statistical indexes of the geoelectric system and earthquakes," *Natural Hazards*, vol. 84, no. 2, pp. 877–895, Nov. 2016.
[41] K. Su, "Earthquake-monitoring capability of borehole strainmeter," (in Chinese), *Earthquake*, vol. 5, pp. 38–46, Oct. 1991.
[42] Z. Qiu, L. Tang, B. Zhang, and Y. Guo, "*In situ* calibration of and algorithm for strain monitoring using four-gauge borehole strainmeters (FGBS)," *J. Geophys. Res., Solid Earth*, vol. 118, no. 4, pp. 1609–1618, Apr. 2013.
[43] M. T. Gladwin and R. Hart, "Design parameters for borehole strain instrumentation," *Pure Appl. Geophys.*, vol. 123, no. 1, pp. 59–80, 1985.
[44] S. M. Pincus and A. L. Goldberger, "Physiological time-series analysis: What does regularity quantify?" *Amer. J. Physiol.-Heart Circulatory Physiol.*, vol. 266, no. 4, pp. H1643–H1656, Apr. 1994.
[45] K. Karamanos, D. Dakopoulos, K. Aloupis, A. Peratzakis, L. Athanasopoulou, S. Nikolopoulos, P. Kapiris, and K. Eftaxias, "Preseismic electromagnetic signals in terms of complexity," *Phys. Rev. E Stat. Nonlinear Soft Matter Phys.*, vol. 74, no. 2, pp. 016104–016125, 2006.
[46] I. Prigogine and I. Stengers, *Order Out Chaos: Man's New Dialogue With Nature*. Brooklyn, NY, USA: Verso Books, 2018.
[47] S. Wiemer and M. Wyss, "Mapping the frequency-magnitude distribution in asperities: An improved technique to calculate recurrence times?" *J. Geophys. Res., Solid Earth*, vol. 102, no. 7, pp. 15115–15128, 1997.
[48] A. Ghosh, A. V. Newman, A. M. Thomas, and G. T. Farmer, "Interface locking along the subduction megathrust from *b*-value mapping near Nicoya Peninsula, Costa Rica," *Geophys. Res. Lett.*, vol. 35, no. 1, pp. 1–6, 2008.
[49] Y. Zhao and Z. Wu, "Mapping the *b*-values along the Longmenshan fault zone before and after the 12 May 2008, Wenchuan, China, Ms 8.0 earthquake," *Natural Hazards Earth Syst. Sci.*, vol. 8, no. 6, pp. 1–11, 2008.
[50] K. Z. Nanjo, N. Hirata, K. Obara, and K. Kasahara, "Decade-scale decrease in *b* value prior to the M9-class 2011 Tohoku and 2004 Sumatra quakes," *Geophys. Res. Lett.*, vol. 39, no. 20, pp. 1–4, Oct. 2012.
[51] W. Xie, K. Hattori, and P. Han, "Temporal variation and statistical assessment of the *b* value off the pacific coast of Tokachi, Hokkaido, Japan," *Entropy*, vol. 21, no. 3, p. 249, Mar. 2019.
[52] K. Aki, "Maximum likelihood estimate of b in the formula log n=a-bm and its confidence limits," *Bull. Earthq. Res. Inst., Tokyo Univ.*, vol. 43, no. 2, pp. 237–239, 1965.
[53] S. Wiemer and M. Wyss, "Minimum magnitude of completeness in earthquake catalogs: Examples from Alaska, the Western United States, and Japan," *Bull. Seismol. Soc. Amer.*, vol. 90, no. 4, pp. 859–869, Aug. 2000.
[54] R. Pawlowicz, B. Beardsley, and S. Lentz, "Classical tidal harmonic analysis including error estimates in MATLAB using T_TIDE," *Comput. Geosci.*, vol. 28, no. 8, pp. 929–937, Oct. 2002.
[55] N. Matsumoto and E. A. Roeloffs, "Hydrological response to earthquakes in the Haibara well, central Japan–II. Possible mechanism inferred from time-varying hydraulic properties," *Geophys. J. Int.*, vol. 155, no. 3, pp. 899–913, Dec. 2003.
[56] Q. Liu, J. Zhang, and S. Chi, "Quality evaluation and fitting analysis of 4-component borehole strainmeter data," (in Chinese), *Earthquake*, vol. 31, no. 2, pp. 87–96, 2011.
[57] W. Marzocchi and D. Melini, "On the earthquake predictability of fault interaction models," *Geophys. Res. Lett.*, vol. 41, no. 23, pp. 8294–8300, Dec. 2014.
[58] A. D. Santis, G. Balasis, F. J. Pavón-Carrasco, G. Cianchini, and M. Mandea, "Potential earthquake precursory pattern from space: The 2015 Nepal event as seen by magnetic swarm satellites," *Earth Planet. Sci. Lett.*, vol. 461, pp. 119–126, Mar. 2017.
[59] V. G. Sibgatulin, S. A. Peretokin, and R. G. Khlebopros, "Fundamental peculiarities of the entropy model of energy processes in seismic areas," *Earth Sci. Frontiers*, vol. 14, no. 6, pp. 222–225, Nov. 2007.

[60] V. Kuksenko, N. Tomilin, E. Damaskinskaya, and D. Lockner, "A two-stage model of fracture of rocks," *Pure Appl. Geophys.*, vol. 146, no. 2, pp. 253–263, Mar. 1996.
[61] D. Lockner, J. Byerlee, V. Kuksenko, A. Ponomarev, and A. Sidorin, "Observations of quasistatic fault growth from acoustic emissions," *Int. Geophys. Ser.*, vol. 51, pp. 3–31, 1992.
[62] Z. Li, S. Ni, T. Hao, Y. Xu, and S. Roecker, "Uppermost mantle structure of the Eastern margin of the Tibetan Plateau from interstation Pn traveltime difference tomography," *Earth Planet. Sci. Lett.*, vols. 335–336, pp. 195–205, Jun. 2012.
[63] X. Zeng, Y. Luo, L. Han, and S. Yaolin, "The Lushan Ms7 earthquake on 20 April 2013: A high-angle thrust event," (in Chinese), *Chin. J. Geophys.*, vol. 56, no. 4, pp. 1418–1424, 2013.
[64] X. Yang, "The stress distribution of the locked region in the fault and its near area," (in Chinese), *North China Earthq. Sci.*, vol. 8, no. 1, pp. 30–37, 1990.
[65] R. E. Kalman, "A new approach to linear filtering and prediction problems," *J. Basic Eng.*, vol. 82, no. 1, pp. 35–45, Mar. 1960.
[66] A. P. Sage and G. W. Husa, "Adaptive filtering with unknown prior statistics," in *Proc. Joint Autom. Control Conf.*, no. 7, 1969, pp. 760–769.
[67] H. Akaike, "A new look at the statistical model identification," *IEEE Trans. Autom. Control*, vol. AC-19, no. 6, pp. 716–723, Dec. 1974, doi: 10.1109/TAC.1974.1100705.
[68] G. Kitagawa and N. Matsumoto, "Detection of coseismic changes of underground water level," *J. Amer. Stat. Assoc.*, vol. 91, no. 434, pp. 521–528, Jun. 1996.
[69] T. Cover and J. Thomas, *Elements of Information Theory*. Hoboken, NJ, USA: Wiley, 1991.
[70] A. Hyvärinen and E. Oja, "Independent component analysis: Algorithms and applications," *Neural Netw.*, vol. 13, nos. 4–5, pp. 411–430, Jun. 2000.
[71] M. C. Jones and R. Sibson, "What is projection pursuit," *J. Roy. Stat. Soc.*, vol. 150, no. 1, pp. 1–37, 1987.

ZINING YU received the bachelor's degree from the College of Instrumentation and Electrical Engineering, Jilin University, Changchun, China, in 2016, where she is currently pursuing the Ph.D. degree. Her current research interests include signal processing, seismic observation data analysis, and seismic precursor analysis.

KAIGUANG ZHU received the Ph.D. degree in earth exploration and information technology from Jilin University, Changchun, China, in 2002. Her current research interests include signal processing involved with airborne electromagnetic survey and earthquake precursor analysis from both ground-based and satellite observations.

KATSUMI HATTORI (Member, IEEE) received the Ph.D. degree in electrical and electronics engineering from Nagoya University, Japan, in 1992. Since 2007, he has been a Professor with the Graduate School of Science, Chiba University. His current research interests include electromagnetic approaches to mitigate natural hazards and to forecast in crustal disasters such as earthquakes, volcano eruptions, and landslides.

CHENGQUAN CHI received the Ph.D. degree from the College of Instrumentation and Electrical Engineering, Jilin University, Changchun, China, in 2020. He has been a Lecturer with the School of Information Science and Technology, Hainan Normal University, Hainan, China. His research interests include blind source separation, geophysics, and signal processing, especially earthquake precursor data.

MENGXUAN FAN received the bachelor's degree from the College of Instrumentation and Electrical Engineering, Jilin University, Changchun, China, in 2017, where she is currently pursuing the Ph.D. degree. Her current research interests include signal processing, seismic precursor anomaly detection, and satellites data processing.

XIAODAN HE received the bachelor's degree from the College of Instrumentation and Electrical Engineering, Jilin University, Changchun, China, in 2019, where she is currently pursuing the master's degree. Her current research interests include signal processing, seismic precursor anomaly detection, and satellites data processing.